Mechanics & Industry **21**, 621 (2020)
© AFM, EDP Sciences 2020
https://doi.org/10.1051/meca/2020095

Mechanics & Industry

Available online at:
www.mechanics-industry.org

Regular Article

Investigation on the effect of leading edge tubercles of sweptback wing at low reynolds number

Veerapathiran Thangaraj Gopinathan[1], John Bruce Ralphin Rose[2,*], and Mohanram Surya[3]

[1] Department of Mechanical Engineering
[2] Department of Mechanical Engineering, Anna University Regional Campus, Tirunelveli627007, India
[3] Hindusthan College of Engineering & Technology, Coimbatore 641032, India

Received: 28 April 2020 / Accepted: 27 November 2020

Abstract. Aerodynamic efficiency of an airplane wing can be improved either by increasing its lift generation tendency or by reducing the drag. Recently, Bio-inspired designs have been received greater attention for the geometric modifications of airplane wings. One of the bio-inspired designs contains sinusoidal Humpback Whale (HW) tubercles, i.e., protuberances exist at the wing leading edge (LE). The tubercles have excellent flow control characteristics at low Reynolds numbers. The present work describes about the effect of tubercles on swept back wing performance at various Angle of Attack (AoA). NACA 0015 and NACA 4415 airfoils are used for swept back wing design with sweep angle about 30°. The modified wings (HUMP 0015 A, HUMP 0015 B, HUMP 4415 A, HUMP 4415 B) are designed with two amplitude to wavelength ratios (η) of 0.1 & 0.24 for the performance analysis. It is a novel effort to analyze the tubercle vortices along the span that induce additional flow energy especially, behind the tubercles peak and trough region. Subsequently, Co-efficient of Lift (C_L), Co-efficient of Drag (C_D) and boundary layer pressure gradients also predicted for modified and baseline (smooth LE) models in the pre & post-stall regimes. It was observed that the tubercles increase the performance of swept back wings by the enhanced C_L/C_D ratio in the pre-stall AoA region. Interestingly, the flow separation region behind the centerline of tubercles and formation of Laminar Separation Bubbles (LSB) were asymmetric because of the sweep.

Keywords: Bio-inspired design / swept back wing / stall / tubercle vortices / L / D optimization

1 Introduction

As novel morphologies and physiological operations are investigated by the biologists, they are serving as a key inspiration for the advancement in technologies. Humpback Whale (HW) (*Megaptera Novaengliae* – great wing of New England) is a stout rorqual in the Balaenopteridae family. The HW is one of the bio-inspired species which is most acrobatic of baleen whales capable of performing high manoeuvres in the underwater environment. The presence of Leading Edge (LE) tubercles in the flipper of HW is used to execute the loops, rolls and banking turn to capture the prey [1]. The hunting tactic of HW is known as horizontal pectoral herding that is possible because of the presence of its flippers. The forelimbs are known as flippers (like wings) which are rounded protuberances or tubercles along the LE of HW that determines the degree of maneuverability. Cooper et al. [2] studied the position of tubercles which is associated with the multiple joints and terminal phalanges from the hyperphalangy of the manus.

The thickness ratio of HW flipper ranges from 0.2 to 0.28 of its chord length while the amplitude of the LE protuberances varies from 2.5% to 12% of the mean chord. Similarly, the wavelength of LE protuberances ranges from 10% to 50% of the mean chord [3]. In recent years, tubercle based modifications on airfoils or wings have received important attention as a passive flow control technique like vortex generators [4]. Tubercle modification can be done based on two geometric parameters namely, the amplitude (A) and wavelength (λ). The strength of rotating vortices created by the tubercles is directly related to the (A/λ) ratio, and modifying this ratio would influence the pattern of vortices [5].

Frank et al. (2011) reported that the effect of flow control caused by the tubercles is strongly associated with the aerodynamic characteristics of lifting surfaces [4]. From this numerical investigation, the simulation of NACA 0021 tubercled wing has revealed 10.9% reduction of induced

* e-mail: bruceralphin@gmail.com

drag because of tubercles. It is also observed that a reduction of circulation gradient exists on the outboard section of wing [6]. Examination by Custadio et al. [7] and Weber et al. [8] highlighted the formation of stream wise counter rotating vortices behind the tubercles. Tuft flow visualization study on a NACA 63_4-021 airfoil with tubercles of different combinations of amplitude and wavelength, shows the lift enhancement, stall angle increment and attached flow behaviours behind the tubercle's peak region for rectangular wings at high Angle of Attack (AoA) [9].

Corsini et al. (2013) investigated the effects of a sinusoidal LE fitted to NACA 0015 and NACA 4415 profiles through OpenFOAM software. The work resulted in the cambered tubercled airfoil recovering earlier during stall phenomenon and has the potential to deliver 25–30% lift increment at post-stall conditions [10]. Later, determination of wake vortex shedding towards the aerodynamic performance enhancement by Large-Eddy Simulation (LES) has been revealed by Percy et al. [11]. Zhang et al. [12] also examined the effects of sinusoidal LE protuberances on a 2D airfoil at the low Reynolds Number (Re) about 5×10^4. Here, it is identified that the function of protuberances is identical to a low-profile vortex generator to a certain degree in the course of boundary-layer separation and control [12]. Later investigation is done as a systematic study about momentum transfer within the boundary layer caused by the strong spanwise pressure gradients, influence of tubercles on the recirculation zone, and wake vortex shedding at low Re [13].

Bolzon et al. [14] observed that the lift and drag levels are reduced for a swept back tubercled wing at lower AoA. Several experiments have been conducted on force measurements with wave survey of smooth and modified wings. From the results, it is highlighted that at lower AoA ($\alpha = 0$–$5°$), LE modification has reduced the Coefficient of lift (C_L) by 4–6% and Coefficient of drag (C_D) by 7–9%. Hence, as an inference the tubercles has increased the Lift to drag (L/D) ratio of swept back tapered wings by 2–6%. Aerodynamic characteristics and surface flow patterns of tubercled tapered swept back wings were analyzed by Wei et al. [15]. It is concluded that the L/D of tubercled tapered swept back wing is lesser than the baseline counterparts in the AoA range from $\alpha = 7°$ to $\alpha = 20°$ for the SD 7032 airfoil at $\mathrm{Re} = 8.2 \times 10^4$.

Bolzon et al. (2016) conducted a wake survey investigation on swept back tapered wings (with NACA 0021 airfoil) at $\mathrm{Re} = 2.25 \times 10^5$. Here, the tubercled wing has produced a higher profile C_D and reduced the induced C_D apparently because of the flow separation adjacent to the wingtip region at $\alpha \geq 9°$. Further, it gives more insights about Laminar Separation Bubble (LSB) distribution, and asymmetric flow separation region behind tubercles trough centerline due to sweep [16]. The effects of LE tubercles on sweptback HW flipper models were experimentally analyzed by Murray et al. [17] and reported the possibility of enhanced aerodynamic performance with increasing sweep angle.

Recently, the breaching behavior and the kinematics of large whales including HW were clearly analyzed by Segre et al. [18]. They found that HW used variable underwater trajectories including upward acceleration and featured a wide range of exiting pitch angles, roll angles, and speeds. Hence, Tubercles on wing LE have the potential to improve the aerodynamic performance of unswept wings. From these multidisciplinary investigations, the present work is proposed to analyze the bio-inspired tubercles from HW on sweptback wings. Empirical and computational analyses have been demonstrated that the LE tubercles passively modify the complete flow field over wing-like structures. In the previous attempt of investigations, rectangular wing planforms with LE tubercles were mainly focused. Implementation of wing sweep has become a popular choice during wing design to achieve higher critical Mach numbers with lower C_D. Therefore, the proposed work is focused with the aerodynamic performance investigation of tubercles on tapered swept back wings at various AoA including the boundary layer pressure gradients. The inspiration of HW manoeuvres at high AoA during feeding in the underwater environment is the driving force behind this proposed work. The outcomes of this investigation may yield significant benefits to commercial airplane aerodynamics, wind turbine blade designs as well as various UAV's applications.

2 Numerical methodology

The overview of numerical analysis methodology used in the proposed work with bio-inspired sinusoidal LE design on the sweptback wing configurations is illustrated in Figure 1.

2.1 Wing geometry

The swept back wing geometry considered for this proposed work is commonly used in various kinds of flight vehicles. Six tapered swept back wings (Baseline A, Baseline B, HUMP 0015 A, HUMP 0015 B, HUMP 4415 A, HUMP 4415 B) are modelled by considering two different airfoils and amplitude to wavelength (A/λ) ratio. Baseline wing model has a smooth LE while the Hump model consists of the tubercles at the LE [16]. The selected NACA 0015 & NACA 4415 airfoils are validated at low Re that is a novel effort to achieve the performance comparison of tubercles over symmetric and cambered wings. The geometric parameters governing the performance of tubercle configurations are wavelength (λ), amplitude (A) and the ratio of amplitude to wavelength, i.e., $\eta = (A/\lambda)$. These geometric parameters would retain the high-priority in the course of design perspective with modified airfoils. The spanwise ordinates (Z) of the geometry for the variable chord length is given by the following wave equation,

$$c(Z) = A\cos\left(\frac{2\pi Z}{\lambda}\right) + \overline{c} \tag{1}$$

Baseline and modified wings are designed with NACA 0015 and NACA 4415 airfoil cross sections respectively. It has a root chord of 100 mm and tip chord of 30 mm, sweep angle about 30° and span is 300 mm. The corresponding

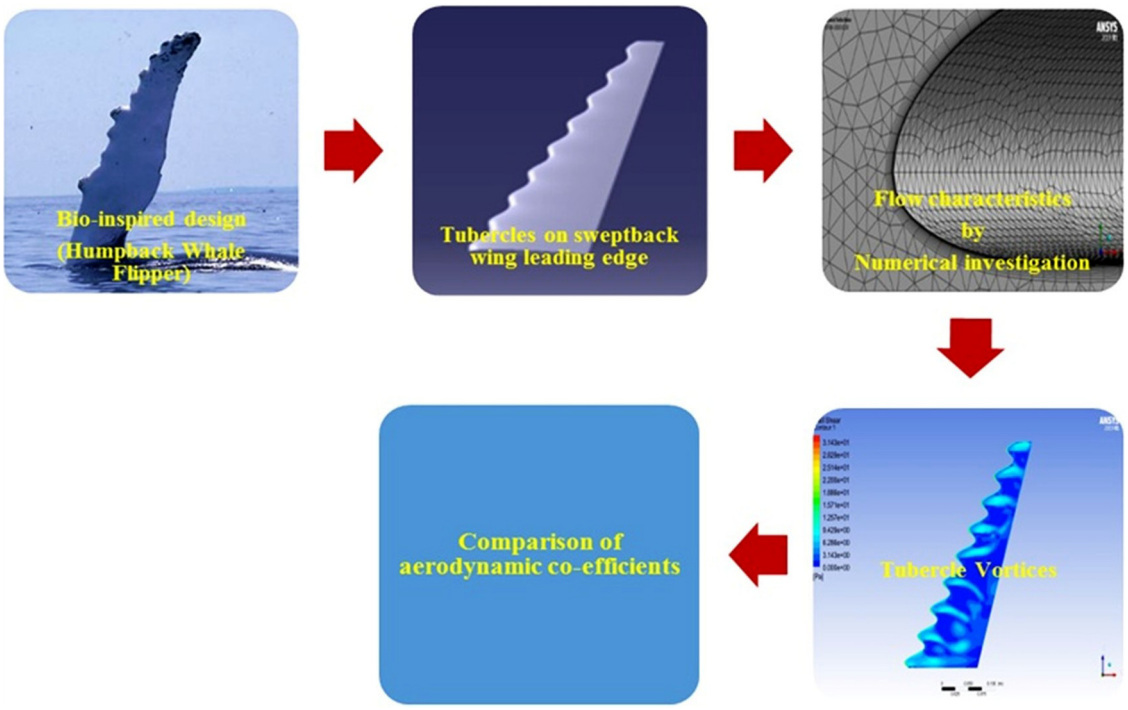

Fig. 1. Analysis methodology of the proposed work.

Fig. 2. CAD model of symmetric wing profiles with tubercles (NACA 0015). (a) Baseline NACA 0015. (b) HUMP 0015 A ($\eta = 0.1$). (c) HUMP 0015 B ($\eta = 0.24$).

mean aerodynamic chord ($\overline{c}$) is determined as 71.28 mm. The modified wings are oriented by implementing the tubercles along the streamwise cross section of the baseline models. Two amplitudes ($A = 0.05\,\overline{c}$ and $0.12\,\overline{c}$) are chosen with one wavelength ($\lambda = 0.5\ \overline{c}$) after the careful examination of various related works. The chosen relative amplitude & wavelength of tubercles on the modified wings in the present work fall within the range of values associated with HW flippers [3]. The Computer Aided Design (CAD) of baseline and tubercled swept back wings with two different η values are presented in Figures 2 and 3 respectively. In this article, the thickness to chord (t/c) value is fixed at 0.15 based on the pectoral flippers existing in the HW as a novel effort compared with the previous studies.

2.2 Computational meshing and numerical simulation

ANSYS Fluent is used to compute the flow field characteristics over the baseline & modified profiles. The mesh generation is done using the method of hybrid grid generation that offers the maximum accuracy in a less computing time. Global mesh, shell mesh, volume mesh and prism layers are selected as pre-mesh parameters for

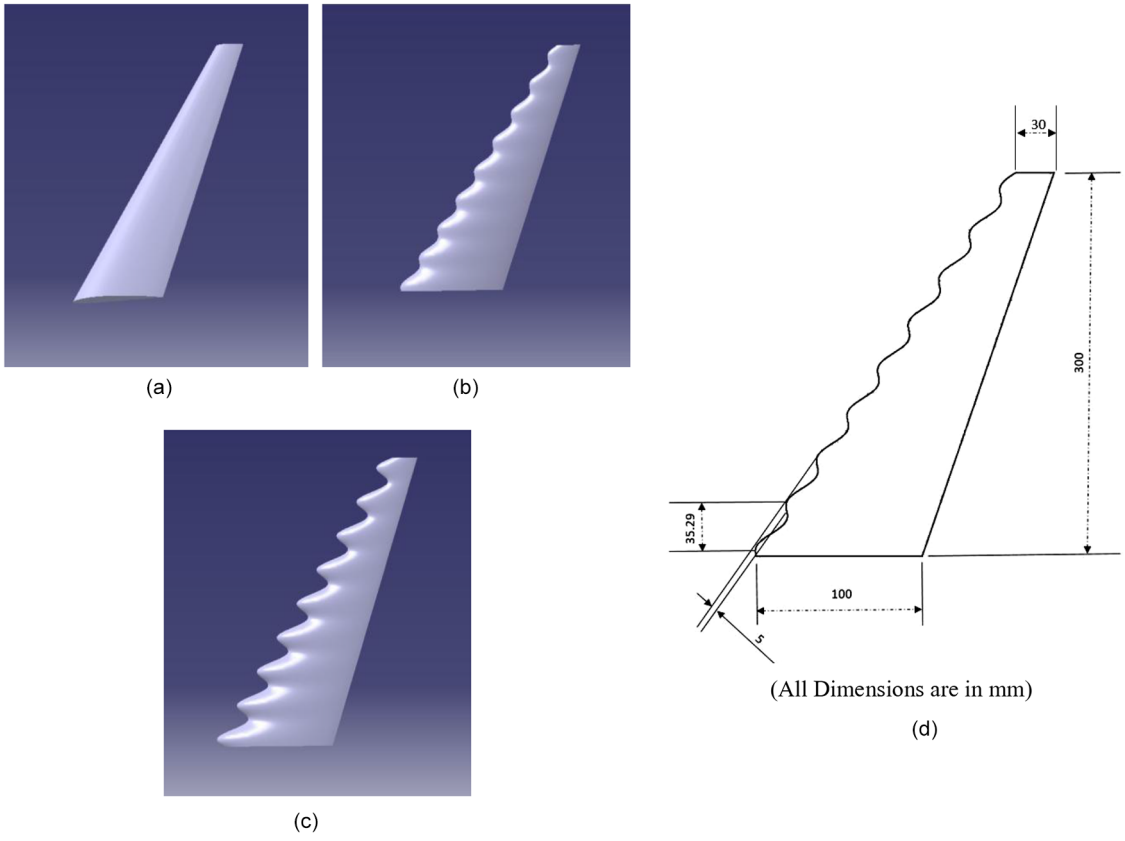

Fig. 3. CAD model of cambered wing profiles with tubercles (NACA 4415). (a) Baseline NACA 4415. (b) HUMP 4415 A ($\eta = 0.1$). (c) HUMP 4415 B ($\eta = 0.24$). (d) Dimensions of CAD model.

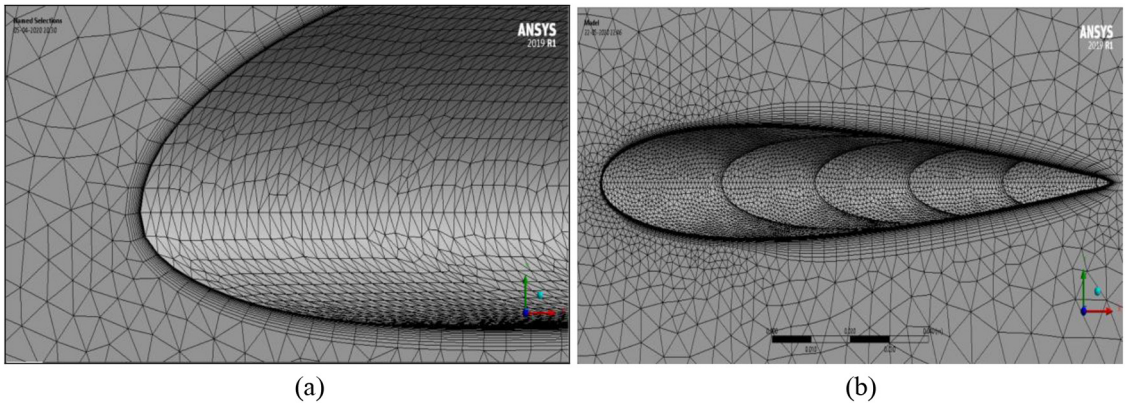

Fig. 4. Prism layer formation in baseline and HUMP airfoil surfaces. (a) Baseline Airfoil. (b) HUMP 0015 B airfoil surface.

meshing the 3D wing geometry. The mesh was constructed with an inflation layer such that the y^+ value is maintained as $y^+ \leq 3$. The maximum element size is restricted at 0.05 and the scale factor is maintained about unity. In the prism layer parameter, the initial height input computed through the y^+ value is about 1.139×10^{-5} as shown in Figure 4. The total number of elements which include surface and volume elements for Baseline NACA 0015, Baseline NACA 4415, HUMP 0015 A, HUMP 0015 B, HUMP 4415 A, HUMP 4415 B are about 1.3×10^6, 1.3×10^6, 1.4×10^6, 1.4×10^6, 1.4×10^6 and 1.4×10^6 respectively.

In order to capture the transverse gradients of the solution such as pressure and velocities within the boundary layer, the inflated prism layer is preferred in the unstructured meshes. An inflation mesh is synonymous with prism layers that are "inflated" from a triangular surface mesh to create high quality geometry-aligned elements capable of resolving the boundary layer growth

Table 1. The results of the mesh-independency study of the tubercled wing at $Re = 183\,000$.

AoA	No. of elements	Spherical domain radius	C_L	C_D
0°	979264	6 $\overline{c}$	0.3332	0.02239
	1320783	10 $\overline{c}$	0.3200	0.02218
	1902808	15 $\overline{c}$	0.3243	0.02945

over the airfoil surface (McMorris and Kallinderis, [19]). In this work, 30 prism layers have been generated over the baseline and tubercled wing models as depicted in Figure 4a and 4b. More prism layers in the viscous sublayer are appropriate for the enhanced wall treatments.

The Shear Stress Transport (SST) $k-\omega$ model has been selected to solve the steady state incompressible Reynolds Averaged Navier-Strokes equation (RANS) equations.

$$\frac{\partial \overline{U}_i}{\partial x_i = 0} \tag{2}$$

$$\frac{\partial \overline{U}_i}{\partial t} + \overline{U}_j \frac{\partial \overline{U}_i}{\partial x_j} + U'_j \frac{\partial U'_i}{\partial x_j} = \overline{f}_i - \frac{1}{\rho}\frac{\partial \overline{p}}{\partial x_i} + \nu \frac{\partial^2 \overline{U}_i}{\partial x_j \partial x_j} \tag{3}$$

Where, ν is Kinematic viscosity, $\overline{f}$- vector expressing the forces, $\overline{U}_j, \overline{p}$, and ρ representing the mean flow quantities of velocity, pressure and density respectively. A spherical domain topology was adopted as a computational domain with far field boundaries located at 10c. Further, wall boundary condition is assigned for two sides of the domain while the remaining domain surface is considered as a pressure far field and the interior of the domain is named as fluid. The AoA has been changed by rotating the free stream velocity component while maintaining constant orientation of the model.

In order to ensure the mesh quality for good rate of convergence, the grid independence study has been performed. The flow separation and tubercle vortex behind the peak & trough can be captured well in the course of pre & post-stall regions through the quality mesh with enough amount of grid independence. The grid independence study was conducted at AoA $\alpha = 0°$ with three different domain radius as listed in Table 1. Finally, the 10 $\overline{c}$ domain radius (mesh elements about 1.3×10^6) was selected for the remainder of this study as the benefits of the slight refinements in the lift and drag coefficients did not outweigh the costs of additional computing time.

3 Results & discussion

The computational model provides the information that reveals the effect of tubercles for baseline and modified wing configurations when analyzed with $Re = 1.83 \times 10^5$. The simulations have been carried out at different AoA ranging from $\alpha = 0°$–$20°$. The role of tubercles in swept back wing configuration is discussed and compared based on wall shear streamline patterns and aerodynamic coefficients with baseline wing configurations.

3.1 For smooth wing (Baseline)

The wall shear streamline patterns of both baseline models are presented in Figures 5 and 6 respectively. Virtually at all AoA, a large amount of LSB forms over the suction side of the smooth wing which can be observed from the blue coloured regions. It is running almost the entire span of the baseline wing configuration. The formation of LSB has been highlighted separately for clarity in Figure 5b. The spanwise line closest to the wing LE indicates the start of the LSB. In the smooth wing (baseline model), the reattachment should be identified from the rear spanwise lines. From Figures 5c and 6d, it is evident that behind the spanwise line presence of large LSB exists at high AoA, hence the flow is more erratic and it indicates that the flow is turbulent.

At lower AoA, the LSB is close to Trailing Edge (TE) of the smooth wing and there will be a decrement in LSB along the chordwise locations as the AoA increases. LSB location can also be measured at the mean aerodynamic chord as a reference. As the flow approaches the frontline of LSB, it starts to move a little bit laterally towards the wing tip (Fig. 6c). After the flow reattaches near to the wing tip, it also starts to follow a curved path slightly towards the wing tip.

3.2 Tubercle vortices (for modified wing configuration)

In rectangular wings with tubercles, Hansen et al. (2016) highlighted that the presence of tubercles leads to an increased flow velocity along the trough region with larger adverse pressure gradients [18]. This in turn causes the boundary layer separation in the trough region at low AoA. It is also noted that the spanwise pressure gradient set up by the tubercles interact with the vorticity distribution thereby leading to a complex flow pattern. For a conventional unswept tubercled wing, the vortex lines are aligned parallel to the LE with positive vorticity. In swept back tubercled configuration, the vortices pattern created by tubercles is asymmetric in nature. Hence, the regions of separation and attachment of flow on the airfoil can be identified from the surface shear contours.

The surface flow topology on the tubercled wing's suction surface over a range of AoA is displayed in Figures 7–10. Behind the trough region of the tubercle, separation occurs much earlier than the peak region [9] as illustrated in Figure 7c. From the simulation results, the LE, TE vortices and wing tip vortex roll up features are identified in the tubercled wing that mainly affects the parasite and induced drag components. Suction side of tubercled swept back wings decelerates the circulation behind the trough region of each tubercle. These illustrative flow circulations are compared with the wall shear lines on the suction surface of tubercled wings. Each circular vortex structure adjacent to a boundary layer detachment

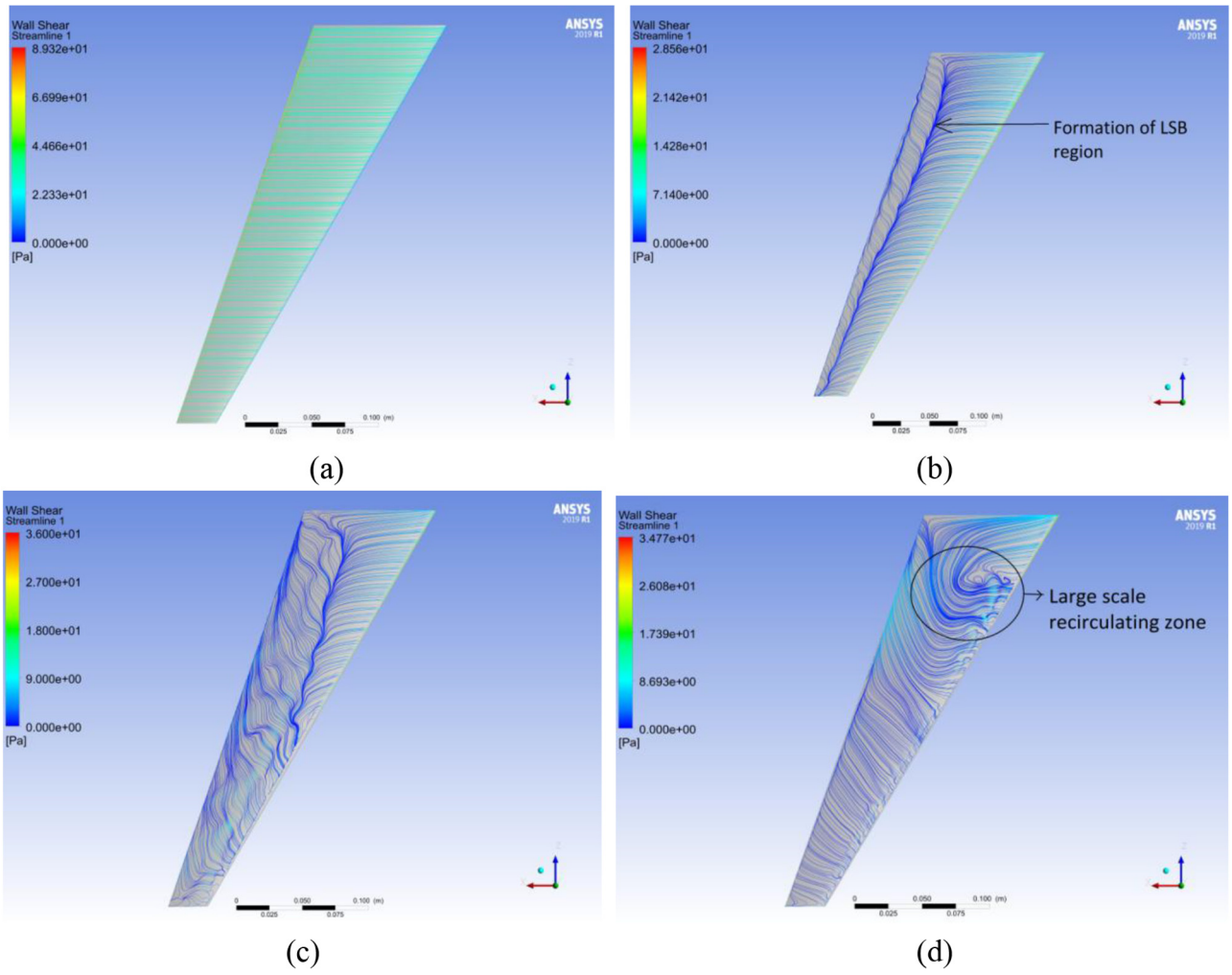

Fig. 5. Wall shear streamline fields over suction side of the baseline wing (NACA 0015) at different AoA. (a) $\alpha = 0°$. (b) $\alpha = 5°$. (c) $\alpha = 10°$. (d) $\alpha = 15°$.

point is observed similar to the procedure followed by Rostamzadeh et al. [20] and Skillen et al. [21]. Hence, it is concluded that the adverse pressure gradient behind the peak region is a crucial reason for the formation of vortex. Further, in the swept tubercled wing configuration, these vortices are asymmetric in size and orientation.

The flow begins to separate significantly over the tubercled wing than the smooth wing configuration at a lower AoA. It is evident by observing the comparison of Figures 5b and 8b at the AoA about 5°. Hence, the flow separates initially behind the troughs of the tubercled wing as displayed in Figures through 7c–10c. Subsequently, the flow separation area enlarges in size proportionate to the incremental AoA as depicted in Figures 7d–10d respectively. Greater adverse pressure gradient is the general motivation for the flow separation behind the trough regions at a lower AoA than the peak regions as compared to the baseline wing. Typically, higher adverse pressure gradient occurs behind the troughs of the tubercles than the peaks of the tubercles as detailed in the literature Hansen et al. [20] and Rostamzadeh et al. [18]. The related works are validated in terms of the qualitative information provided with the outcomes of the numerical analysis as discussed.

At the TE of the wing, a pair of secondary vortices is appeared as shown in Figures 7c and 7d to Figures 10c and 10d respectively. It is being formed beneath the primary vortex pair and at the lower AoA, this pattern is indistinct. At larger AoA ($\alpha = 10°$, 15°), the structure of secondary vortices is more clearly manifested adjacent to the TE. It is also essential to note that the change of tubercle amplitude varies the flow structure over the surface especially, at lower AoA. Figures 9b and 10b illustrate the effect of increased A/λ ratio ($\eta = 0.24$) that makes the flow remain attached at lower AoA. As the AoA increases, there is a modification in the primary and secondary vortices zone because of the change of amplitude as highlighted in Figures 7d and 8d respectively. The surface contours show that a large flow separation zone is formed ahead of the pair of Foci (F), into which the flow spirals.

As the AoA increases, the flow detachment point moves towards the LE as presented in Figure 11 (for AoA, $\alpha \geq 5°$). Preferably, at higher AoA ($\alpha = 15°$), no vortex detachment points are visible behind the trough region that is adjacent

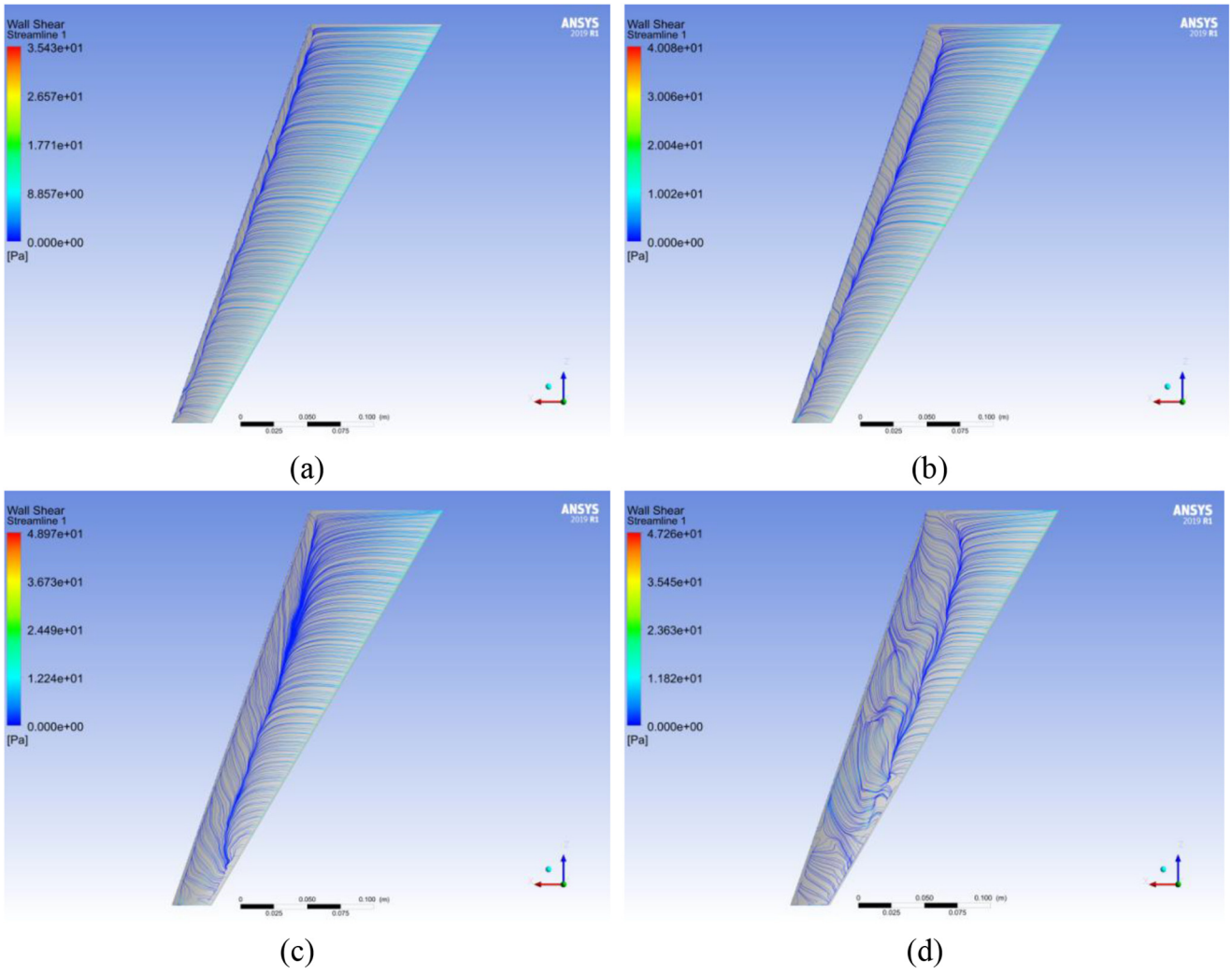

Fig. 6. Wall shear streamline fields over suction side of the baseline wing (NACA 4415) at different AoA. (a) $\alpha = 0°$. (b) $\alpha = 5°$. (c) $\alpha = 10°$. (d) $\alpha = 15°$.

to the wing tip. Moreover, vortex detachment points are identified behind each tubercle's trough region as highlighted in Figure 11.

3.3 Streamline patterns for baseline & modified wing configurations

The flow detachment and formation of LSB can be captured well through the sectional view of velocity streamline patterns at various AoA. Since the overall flow structure over the wing surface is already discussed above, the detailed flow separation characteristics near the stall AoA is considered for the streamline patterns. At $\alpha = 15°$, the velocity streamline patterns over the baseline and tubercled models are presented in Figures 13–18. In the tubercled models (HUMP 0015 & HUMP 4415), the streamlines are visualized at three spanwise locations (along the peak, mid and trough regions) at the distance of 150, 160 and 170 mm respectively from the root chord. The geometric considerations for the analysis of streamline patterns are illustrated in Figure 12. Further, similar locations have been considered for the baseline models as well.

In order to evaluate the influence of tubercles over the smooth LE baseline wings, the streamline patterns are captured from peak, mid and trough regions along the span as specified in Figure 12. At lower AoA, the flow remains fully attached over the suction and pressure surfaces in the range of specified *Re*. As the AoA increases, the flow separation starts at the suction side because of the adverse pressure gradients., At $\alpha = 15°$, major portion of suction surface of both baseline wing models are subjected to separated flow with the primary vortex attached to the suction side and a counter rotating secondary vortex stays behind as illustrated in Figures 13 and 16 [22]. In Figures 14 and 15, the streamlines are illustrated for two different A/λ ratios with symmetric profile based models. Around the tubercled mid and peak regions of HUMP 0015 A, and the trough region of HUMP 0015 B, large scope of flow separation can be observed. However, the flow separation is

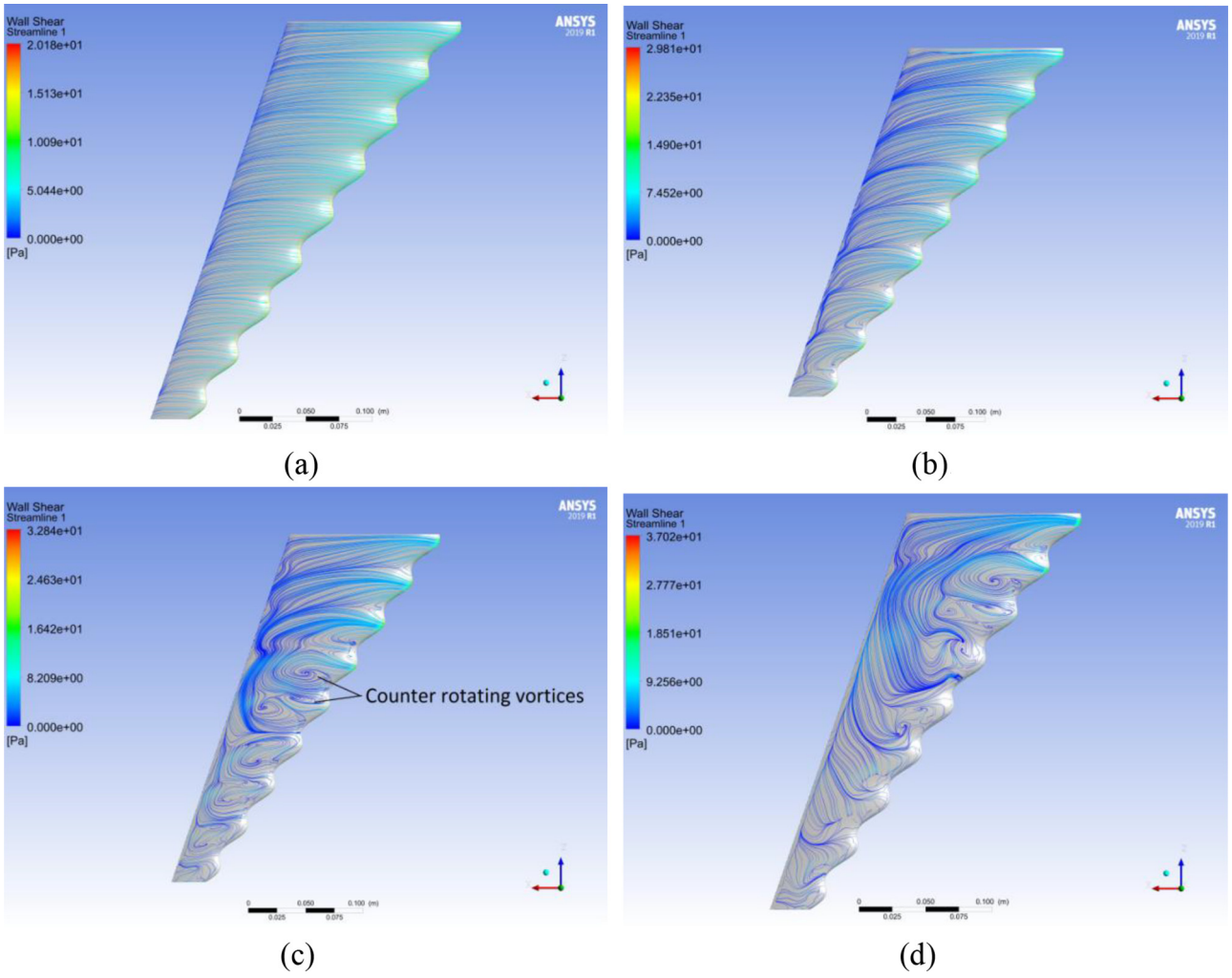

Fig. 7. Wall shear streamline fields over HUMP 0015 A ($\eta = 0.1$) at different AoA. (a) $\alpha = 0°$. (b) $\alpha = 5°$. (c) $\alpha = 10°$. (d) $\alpha = 15°$.

marginally under control along the peak region of the tubercled models due to the presence of counter rotating vortices [21] as highlighted in Figures 14b and 15b respectively.

The stream line patterns of cambered profile (NACA 4415) based modified wings are presented in Figures 17 and 18 respectively. At higher AoA, strong flow separation is observed and the flow separation bubble is quite prominent to cause significant velocity gradients in the boundary layer. Moreover, it is evident that the flow separation behaviour along the suction surface is better at the peak plane than the trough plane. The massive flow separation from the LE causes the formation of LSB at a certain distance in the trough plains. The comparatively higher velocity amplitude shows good flow control, especially in the mid and peak regions as displayed in the Figures 15a and 15b and 18a and 18b respectively. Most of the peak planes of tubercled models demonstrate the flow separations that start adjacent to the mid-chord location (Johari et al., [9]). Hence, the streamline patterns roughly vary along the spanwise direction because of the change of sweep angle and chord with asymmetric vortex structure behind the tubercles.

The implementation of tubercles on sweptback wings with $t/c = 0.15$ has notable effects on the distribution of vortices behind the peak, mid and trough regions. As tubercles delay stall and improve the flow control characteristics, their implementation on flight vehicles would replace the devices incorporated at the LE & TE of airplane wings to achieve boundary layer control (Refer Fig. 15 and 18). The replacement of boundary layer control devices (e.g. LE slots, tabs and auxiliary flaps) with their associated mechanical components could reduce the overall weight of the flight vehicles and improve the fuel economy. Similarly, the Unmanned Aerial Vehicle (UAV) is easily stalled at lower AoA and the stall delay characteristics of tubercled wings with higher L/D at low Re would enhance its performance.

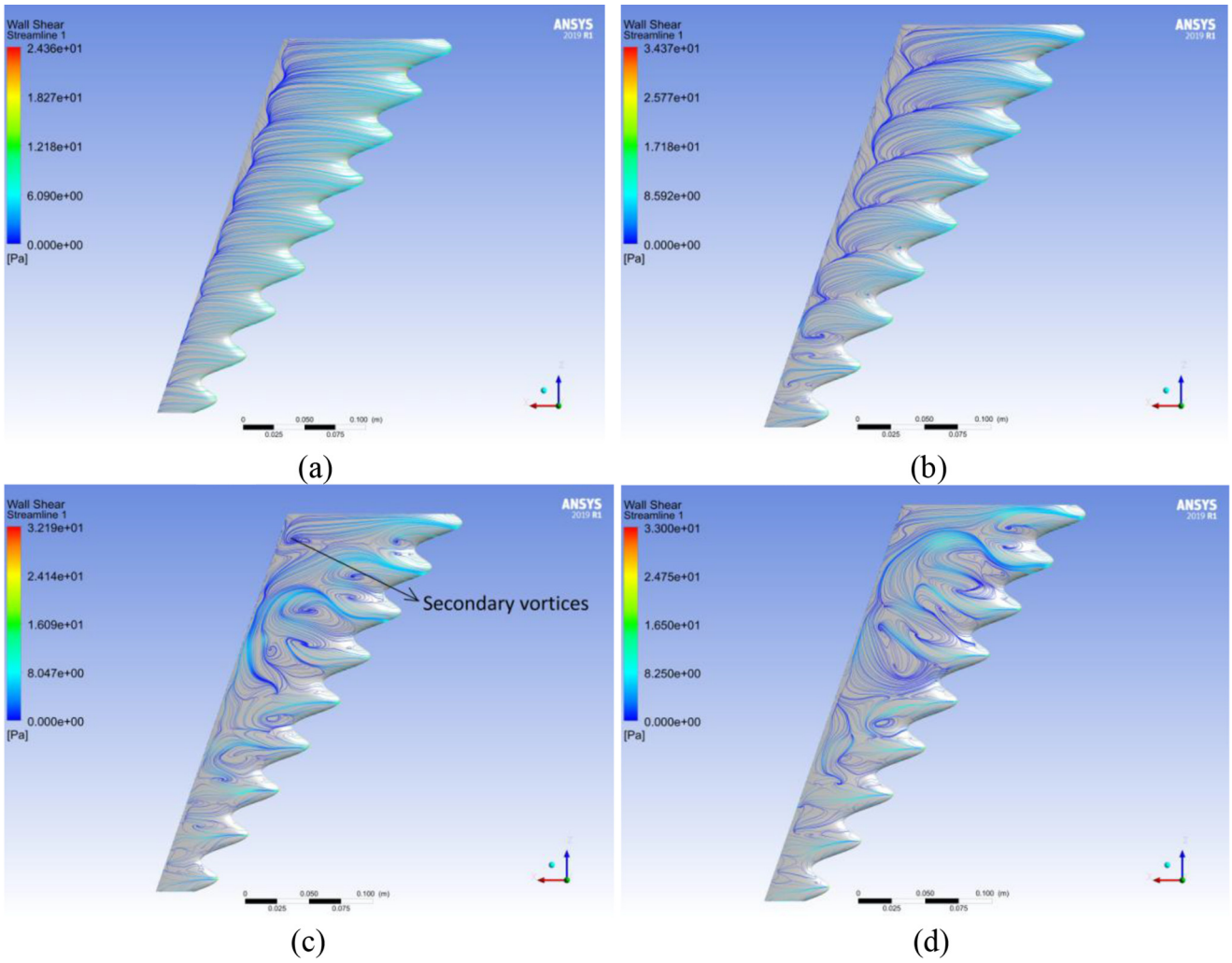

Fig. 8. Wall shear streamline fields over HUMP 0015 B ($\eta = 0.24$) at different AoA. (a) $\alpha = 0°$. (b) $\alpha = 5°$. (c) $\alpha = 10°$. (d) $\alpha = 15°$.

3.4 Effect of tubercles on aerodynamic coefficients

The C_L and C_D computed for the two groups of wings (with NACA 0015 & NACA 4415 airfoils) at the aforesaid Re through the CFD solver at various ($\alpha = 0°$ to $\alpha = 20°$) AoA have been plotted in Figures 19–22. The basic wing configurations presented herewith are classified as symmetric and cambered airfoil profiles. The C_L value at 0° AoA for symmetric profile is close to zero but not exactly zero (Fig. 11). For a cambered wing profile, it is a well-known fact that the zero-lift occurs at some specific negative AoA according to the camber and geometric features of the airfoil. Hence, for the NACA 4415, the computed C_L at 0° AoA is about 0.35 as highlighted in Figure 22. The C_L curves corresponding to the baseline wings show the linear increment in proportion to AoA up to $\alpha = 10°$ with reasonable flow separation at $\alpha \geq 5°$). As the AoA increases above 10°, the C_L distribution becomes nonlinear and gradually rises up to $\alpha \leq 15.5°$ as shown in Figures 19 and 21. However, the C_L reaches the maximum values (at the stalling AoA) of $C_L)_{@\,\alpha=16°} = 0.62$ and $C_L)_{@\,\alpha=14°} = 1.17$ for baseline NACA 0015 and NACA 4415 wings respectively. Afterwards, during the post-stall AoA C_L gradually decreases and the losses in lift are quite moderate for the baseline configurations.

Alternatively, for the tubercled wings, Figures 19 and 21 shows that the stall angles for HUMP 0015 A, B and HUMP 4415 A, B (i.e., $\eta = 0.1$ & $\eta = 0.24$) wings have been reached at $\alpha = 18°$ and $\alpha = 17°$ respectively. It is also apparent that increments in C_L values exist for modified profiles in the pre-stall and post-stall regions (Fig. 19). Further, the C_L value obtained for the tubercled wing is about 10% higher than the C_L of baseline wings. On the comparison of modified profiles, high amplitude tubercled wing (HUMP 0015 B) offers slight increment in C_L at the pre-stall as well as post-stall regions [9]. The camber based modified wing (NACA 4415) shows the reduction in C_L however, delaying the stall characteristics as depicted in Figure 21. This crucial stall delay is achieved because of the deterioration of LSB associated with the leading-edge tubercles [5].

The condition for minimum power required in the course of steady level flight is fulfilled by achieving maximum $C_L{}^{3/2}/C_D$. Hence, the drag performance of the

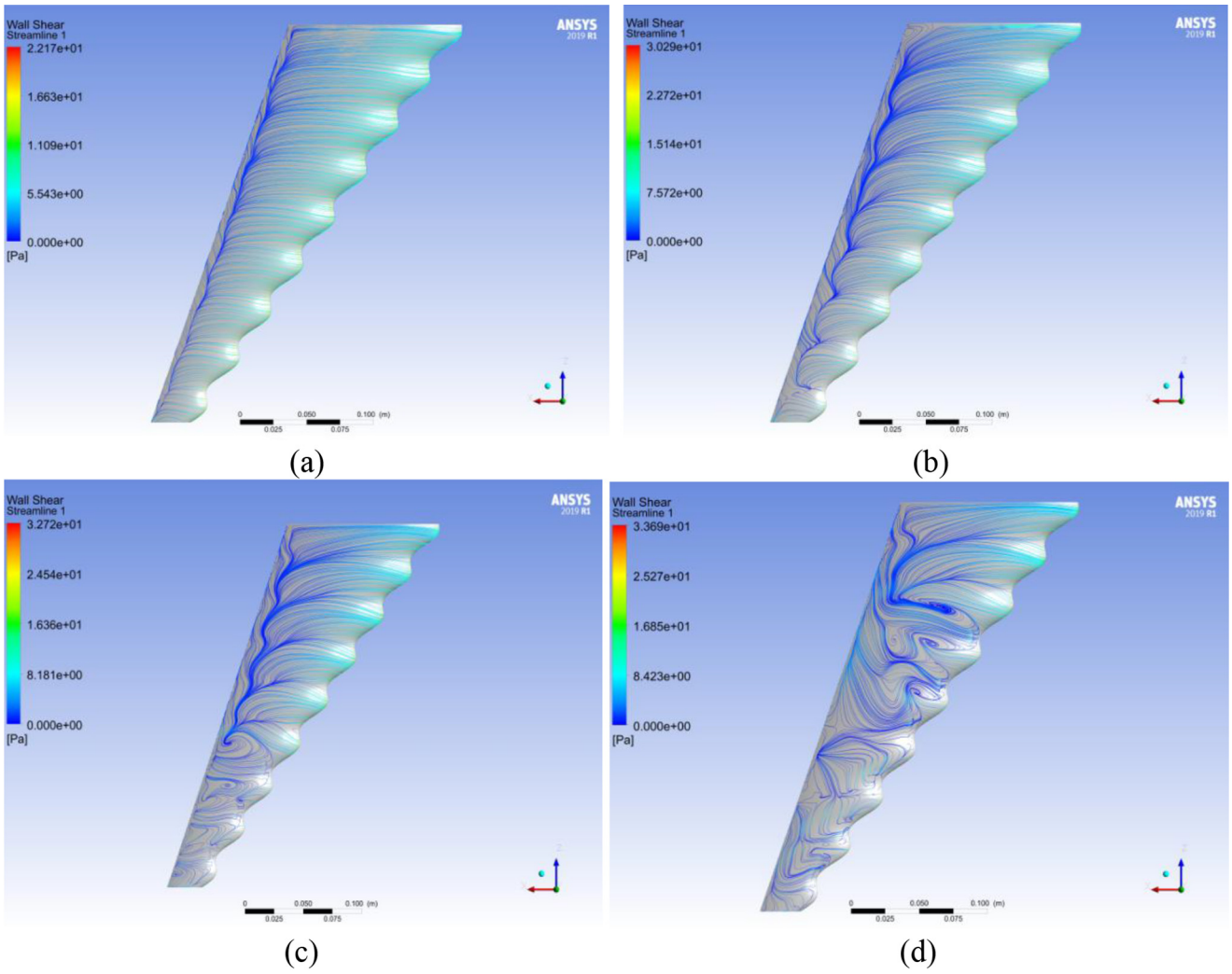

Fig. 9. Wall shear streamline fields over HUMP 4415 A ($\eta = 0.1$) at different AoA. (a) $\alpha = 0°$. (b) $\alpha = 5°$. (c) $\alpha = 10°$. (d) $\alpha = 15°$.

wing is also essential simultaneously with better lifting characteristics over the given range of Re [23]. The two baseline wings with different tubercled airfoil profiles are compared herewith for the effective C_D at various AoA. In the post-stall region ($\alpha > 15°$), the baseline wings are registered with a steep increase in C_D without any change of slope. In the modified tubercled wings, significantly higher C_D level is incurred than the baseline wings as AoA increases above $\alpha = 5°$ and up to $\alpha = 20°$. Figures 19 and 21 highlighted that, the C_D value for both modified profiles ($\eta = 0.1$ & $\eta = 0.24$) increases in a bilinear fashion for the range of AoA $\alpha = 5°$ to $\alpha = 15°$ [24]. It is interesting to note that the slope of the curve increases little by little up to $\alpha = 10°$ and offers a minimum C_D with more than 15% lift at the equivalent AoA as displayed in Figure 12 (symmetric airfoil).

Conversely, from the bilinear nature of the C_D vs. α curve, it is also inferred that the higher AoA (i.e., $\alpha > 10°$) delays the stall with reasonable increment in C_D. Earlier investigations by Miklosovic et al. [25] and Bolzon et al. [26] revealed that the linear increase is likely to be caused by the gradual flow separation behind the tubercle's trough regions where a greater amount of adverse pressure gradient exists. From the C_L and C_D results, the modified wings with $\eta = 0.24$ have the potential to achieve excellent L/D ratio in the pre-stall region because of comparatively smaller LSB being created in the AoA particularly between $\alpha = 0°$ and $\alpha = 10°$.

The drag polar depicted in Figure 23 shows the C_L and C_D variations of baseline and modified profiles at AoA ranging from $\alpha = 0°$ to $\alpha = 20°$. It is observed that at low AoA, the Lift-to-Drag ratio (L/D) values are approximately in close proximity for the smooth LE baseline and tubercled models. As the AoA increases, the L/D ratio of swept back tubercled wing increases in the symmetric case and vice versa [27]. In both the symmetric and cambered profile based wings, as the value of η is increased to $\eta = 0.24$, the models have reasonably good L/D ratio in the pre-stall region. Hence, the empennage part of UAV or airplanes can be optimized with the symmetric case and the primary lifting surfaces should be customized with the cambered tubercled designs. However, the airplane or UAV configuration and mission also must be taken into account prior to the conceptual design phase itself to incorporate

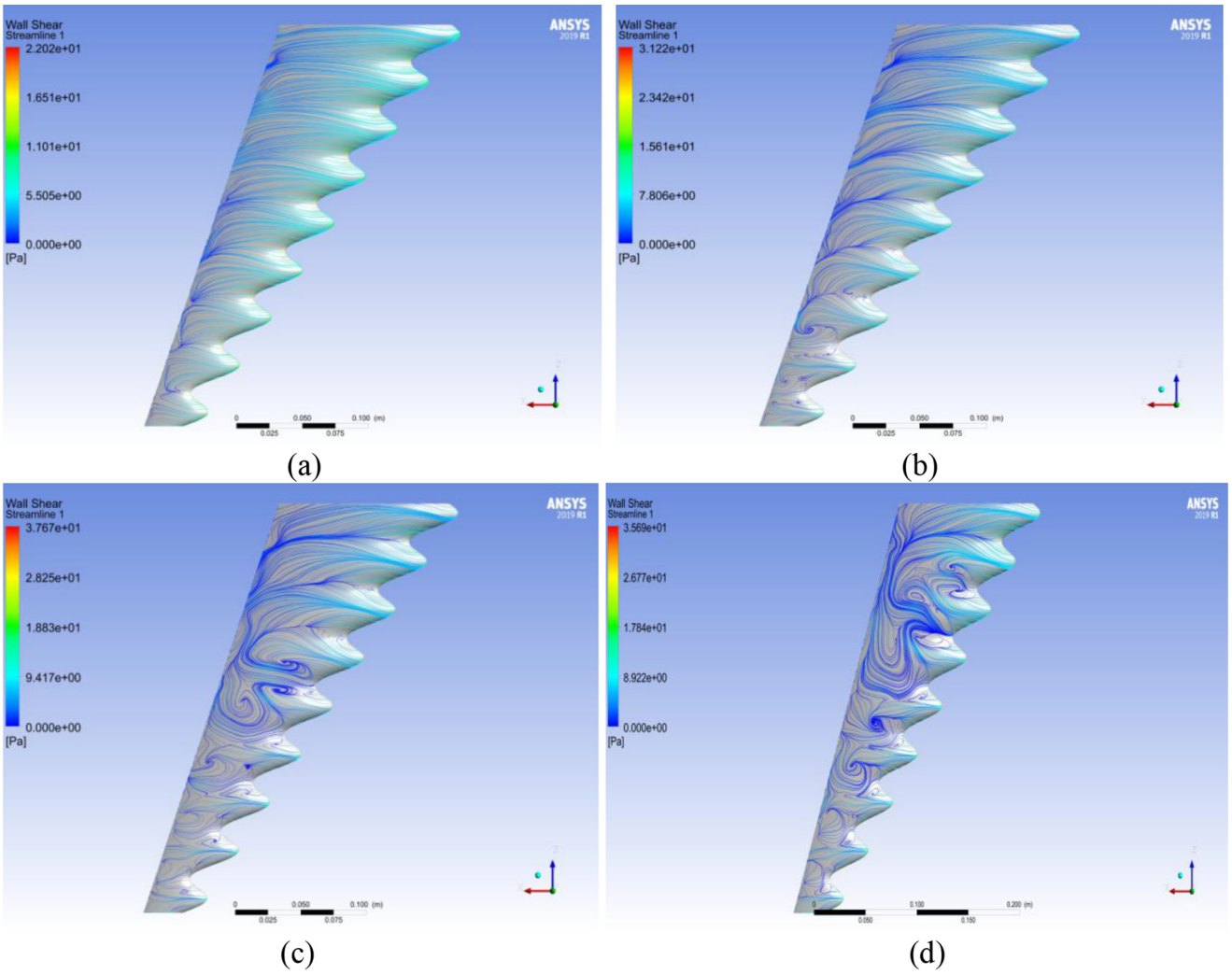

Fig. 10. Wall shear streamline fields over suction side of the HUMP 4415 B ($\eta = 0.24$) at different AoA. (a) $\alpha = 0°$. (b) $\alpha = 5°$. (c) $\alpha = 10°$. (d) $\alpha = 15°$.

such details. In addition to this, it is good to mention that the tubercles with increased A/λ (i.e., $\eta = 0.24$) reduces the noise level significantly in the turbine and compressor blades (Lau et al. [28]).

3.5 Effect of tubercles on boundary layer separation

The presence of tubercles has strong influence in the boundary layer separation characteristics of airplane wings. Here, the flow separation characteristics of baseline (NACA 0015) configuration is compared with the modified (HUMP 0015B) airfoil at two AoA, $\alpha = 5°$ & $15°$ respectively. Typically, to reduce the boundary layer drag, the flow control over the wing surface should be optimized towards favorable pressure gradient for the given AoA and *Re*. The active flow control strategies help to delay the onset of boundary layer transition from laminar to turbulent that is one of the ways to delay the stall phenomenon at high AoA. However, the common active and passive flow control devices integrated to aircraft wings such as vortex generators, winglets, turbulators, and wing fences would cause additional instrumental complexities with detailed maintenance requirements as stated by Bolzon et al. [29]. Hence, in the present work is devised to investigate the feasibility of bio-inspired tubercles to achieve flow control over a range of AoA in a sweptback wing configuration.

The flow separation phenomenon is typically caused by excessive momentum loss adjacent to the wall where the boundary layer tries to move downstream against the increasing pressure (adverse pressure gradient). Hansen et al. (2016) studied the alternate case of decreasing pressure that is known as favorable pressure gradient, where the flow separation is negligible. The velocity vector for the NACA 0015 model with boundary layer profile at the AoA $\alpha = 5°$ is presented in Figure 24. Here, the favorable pressure gradient can be observed up to 60% of the chord from LE, and the flow separation begins afterwards that causes the adverse pressure gradient with a recirculation zone adjacent to the TE.

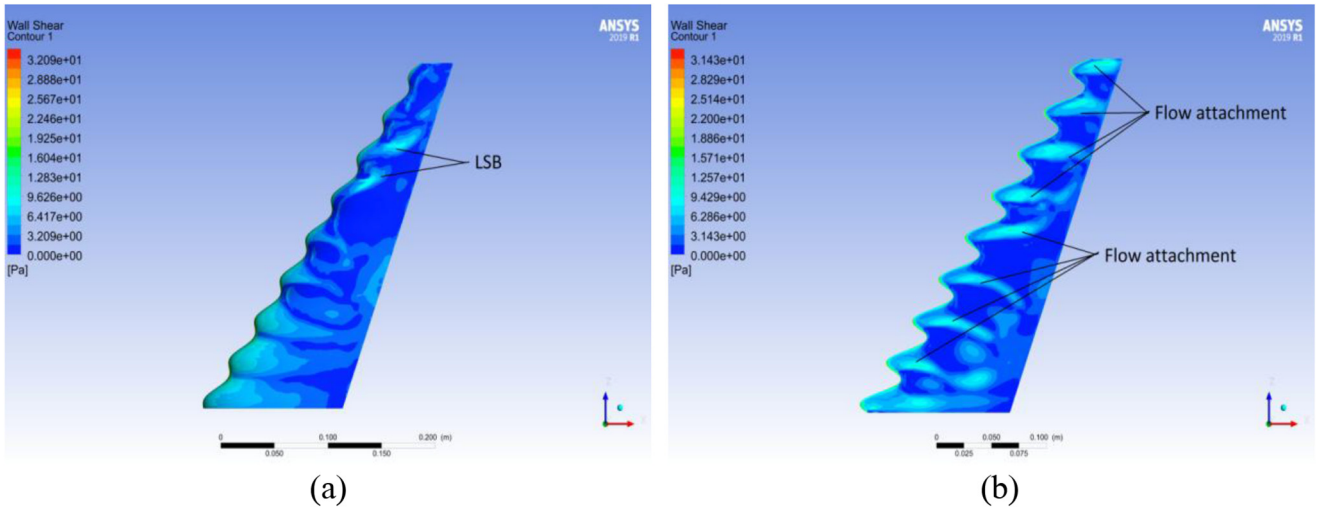

Fig. 11. CFD results depicting LSB and Flow attachment zone for HUMP 0015 at $\alpha = 10°$. (a) Formation of LSB. (b) Flow attachment zone.

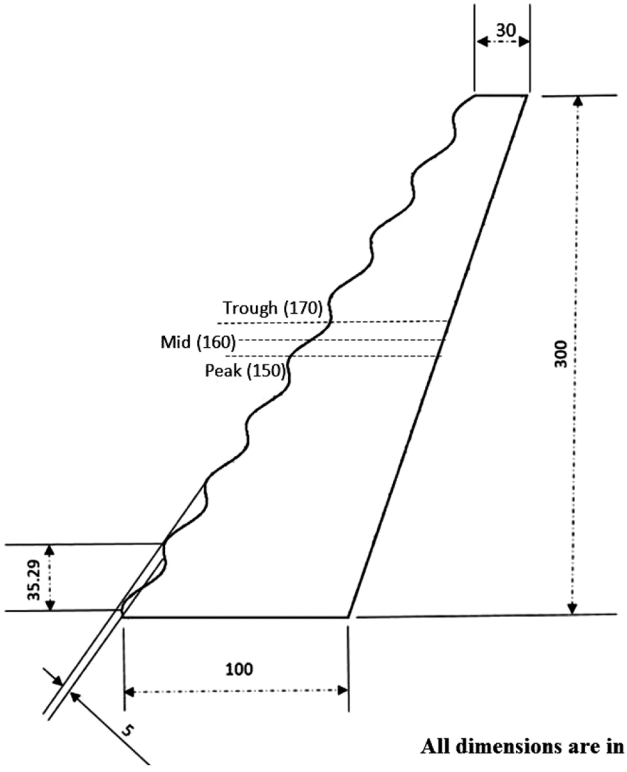

Fig. 12. Schematic diagram of peak, trough and mid-regions of sweptback tubercled model.

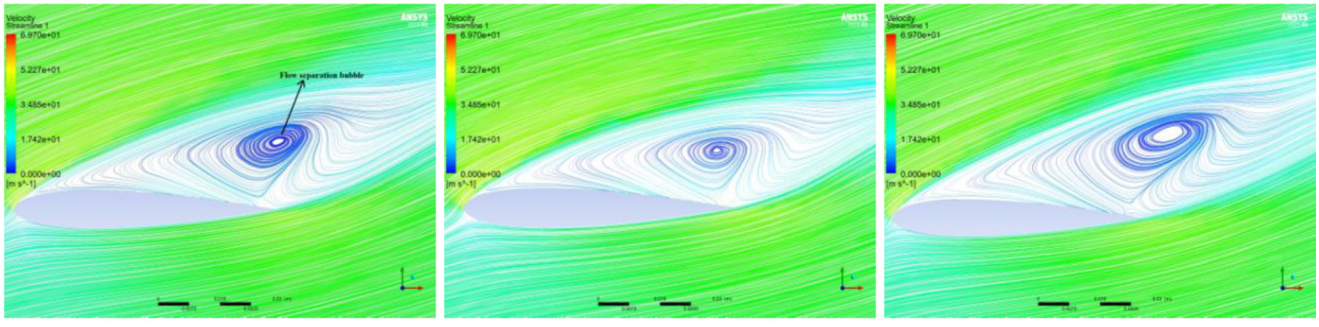

Fig. 13. Streamline pattern over NACA 0015 at different spanwise locations at $\alpha = 15°$. (a) at 160 mm. (b) at 150 mm. (c) at 170 mm.

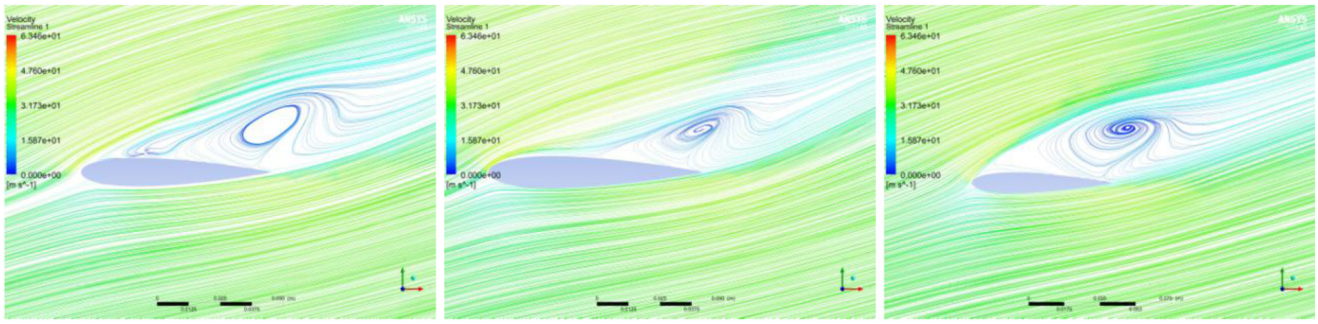

Fig. 14. Streamline fields over HUMP 0015 A at different regions at $\alpha = 15°$. (a) Mid region of HUMP 0015 A. (b) Peak regon of HUMP 0015 A. (c) Trough region of HUMP 0015 A.

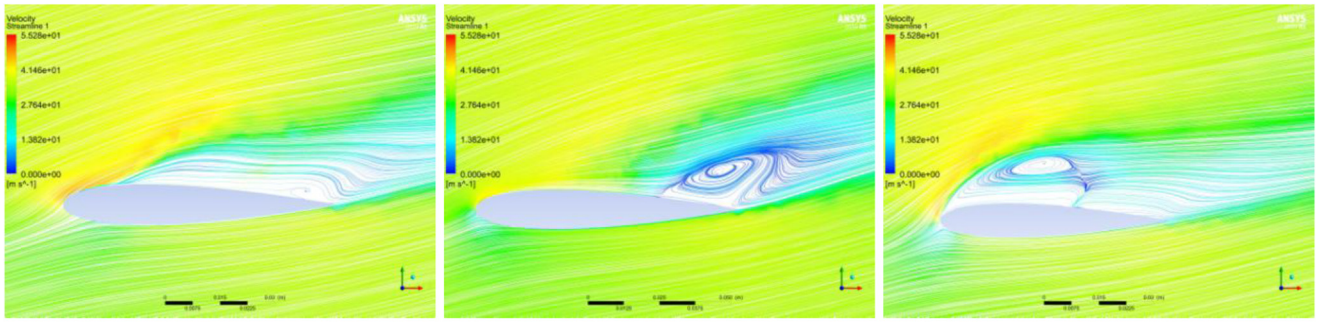

Fig. 15. Streamline fields over HUMP 0015 B at different regions at $\alpha = 15°$. (a) Mid region of HUMP 0015 B. (b) Peak regon of HUMP 0015 B. (c) Trough region of HUMP 0015 B.

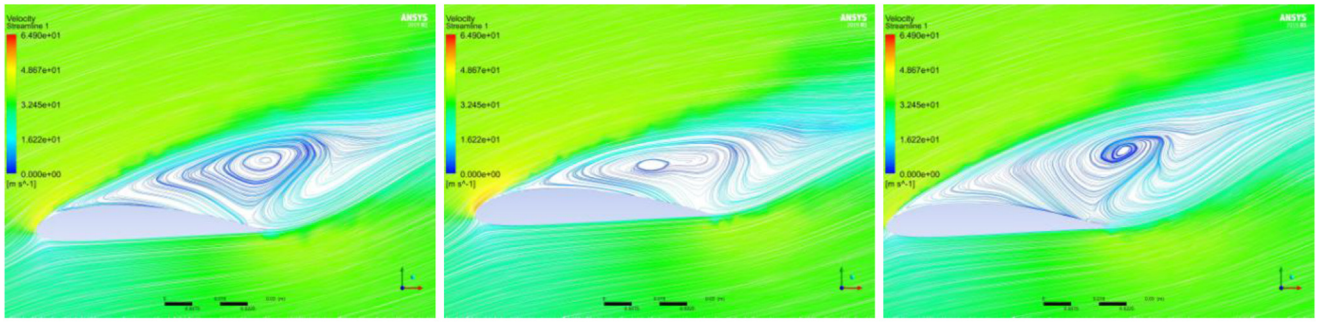

Fig. 16. Streamline fields over NACA 4415 at different span wise locations at $\alpha = 15°$. (a) at 160 mm. (b) at 150 mm. (c) at 170 mm.

The more detailed view of the flow separation zone corresponding to the baseline model is displayed in Figure 25. When an adverse pressure gradient exists, a point of inflection occurs in the boundary layer, and its distance from the wall increases for strong pressure gradients. At the moderate level pressure gradients, the point of inflection is moved in a vertical direction and the critical condition is reached where the wall shear is exactly zero and it is called as flow separation point. In excessive adverse pressure gradients, a reverse flow exists adjacent to the wall that is clearly indicated in Figure 25.

The discussion on effect of tubercles in boundary layer separation is summarized with the comparison of baseline NACA 0015 airfoil with HUMP 0015B configuration at higher AoA. At the AoA $\alpha = 15°$, the flow starts to separate more over the baseline wing, i.e., instantly after the LE of

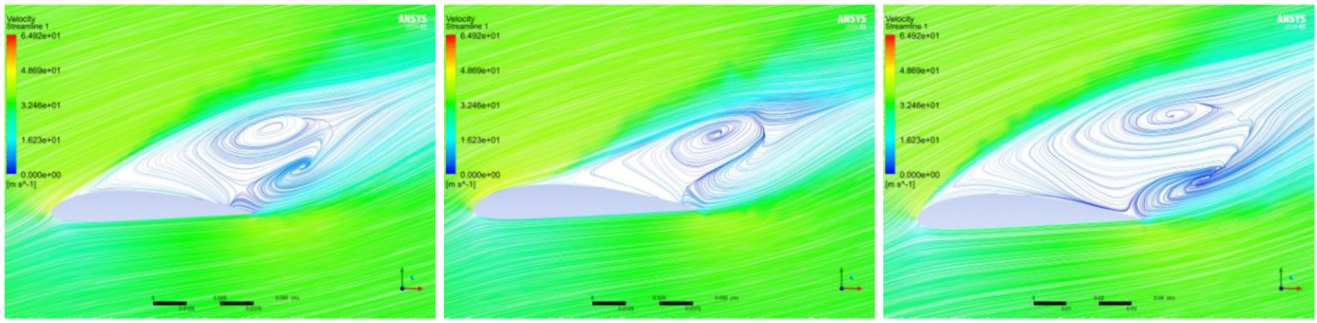

(a) (b) (c)

Fig. 17. Streamline fields over HUMP 4415 A at different regions at $\alpha = 15°$. (a) Mid region of HUMP 4415 A. (b) Peak regon of HUMP 4415 A. (c) Trough region of HUMP 4415 A.

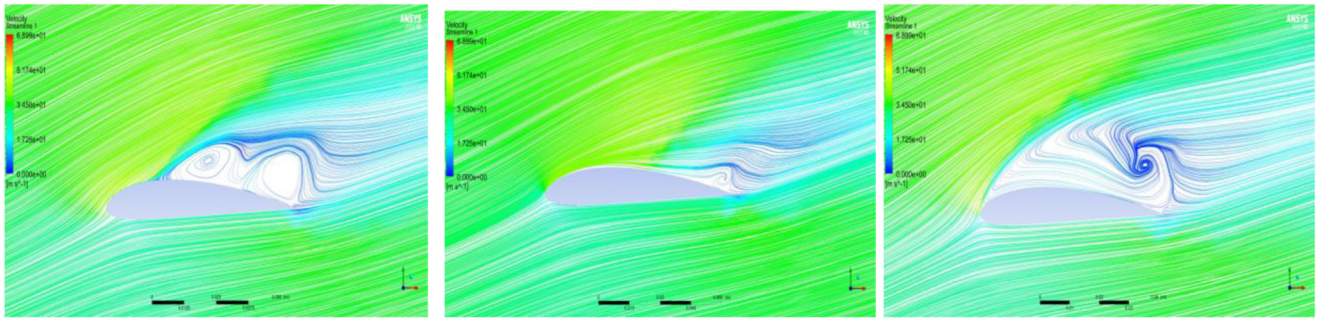

(a) (b) (c)

Fig. 18. Streamline fields over HUMP 4415 B at different regions at $\alpha = 15°$. (a) Mid region of HUMP 4415 B. (b) Peak regon of HUMP 4415 B. (c) Trough region of HUMP 4415 B.

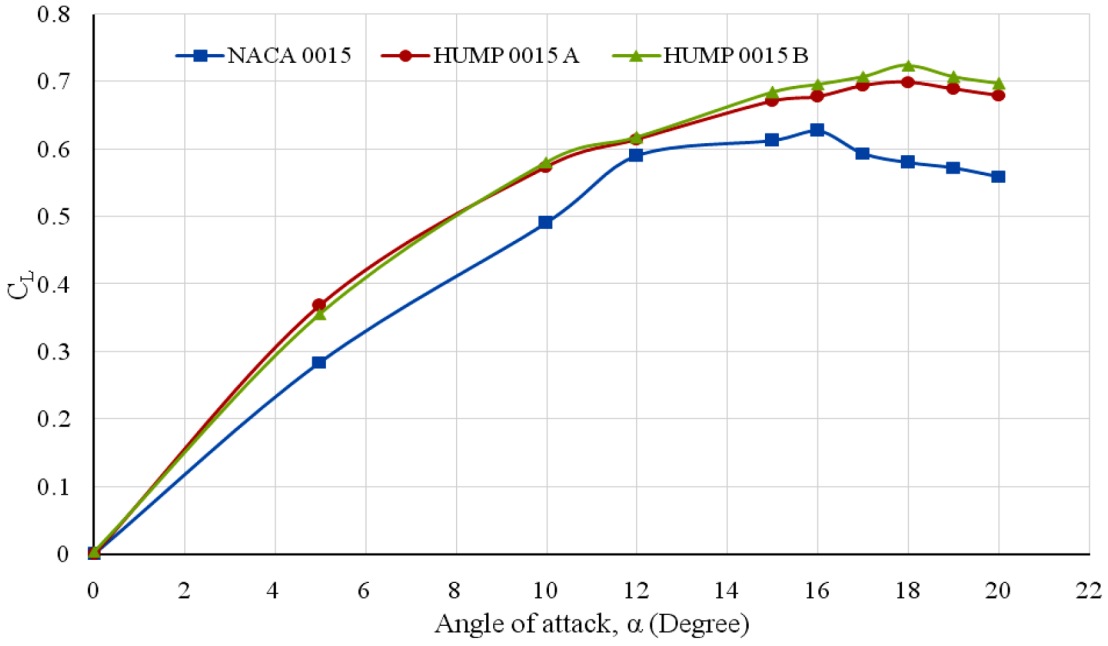

Fig. 19. Comparison of C_L vs. α at different AoA for NACA 0015 case.

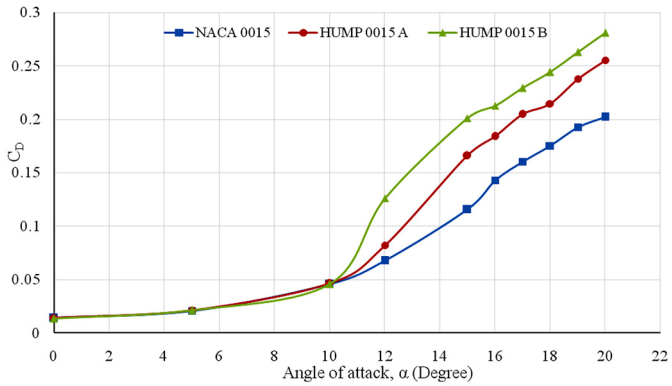

Fig. 20. Comparison of C_D vs. α at different AoA for NACA 0015 case.

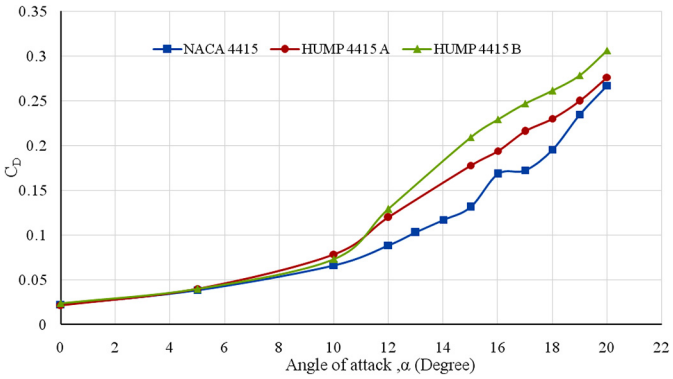

Fig. 22. Comparison of C_D vs. α at different AoA for NACA 4415 case.

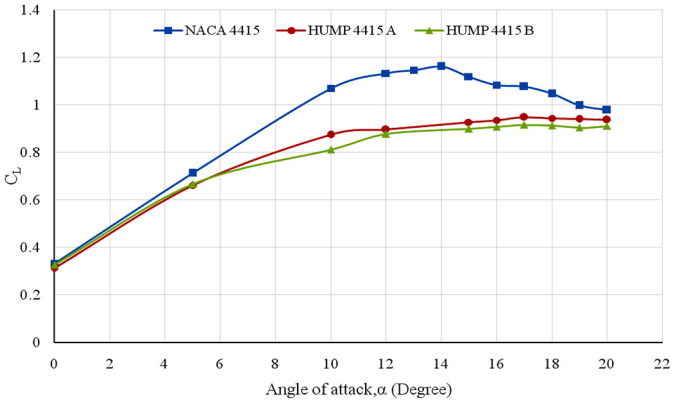

Fig. 21. Comparison of C_L vs. α at different AoA for NACA 4415 case.

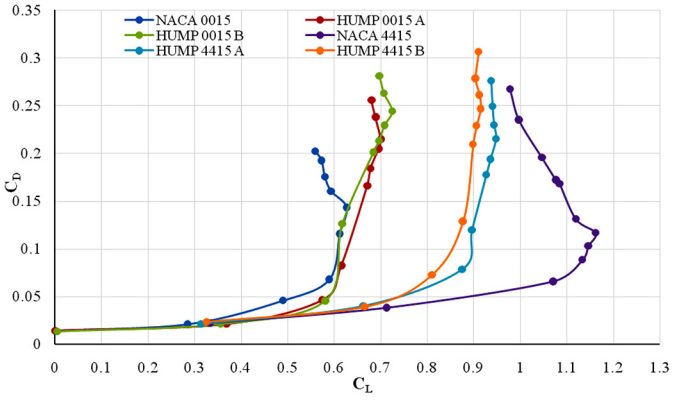

Fig. 23. Comparison of smooth LE and tubercled drag polar for sweptback wings.

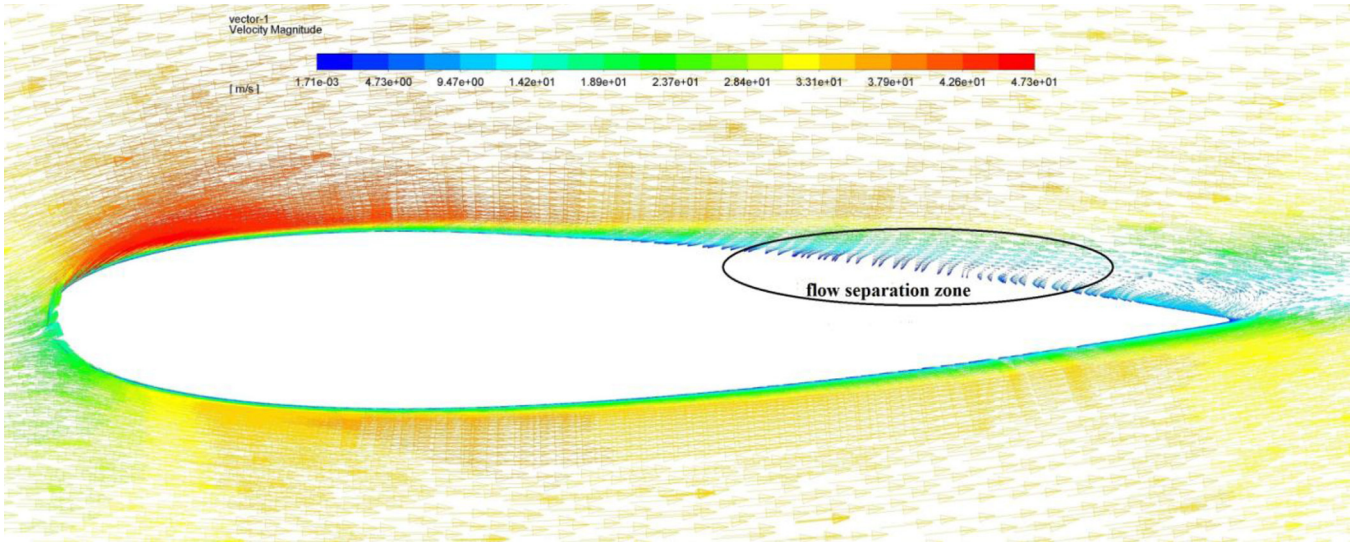

Fig. 24. Velocity vector with boundary layer profile for NACA 0015 model at $\alpha = 5°$.

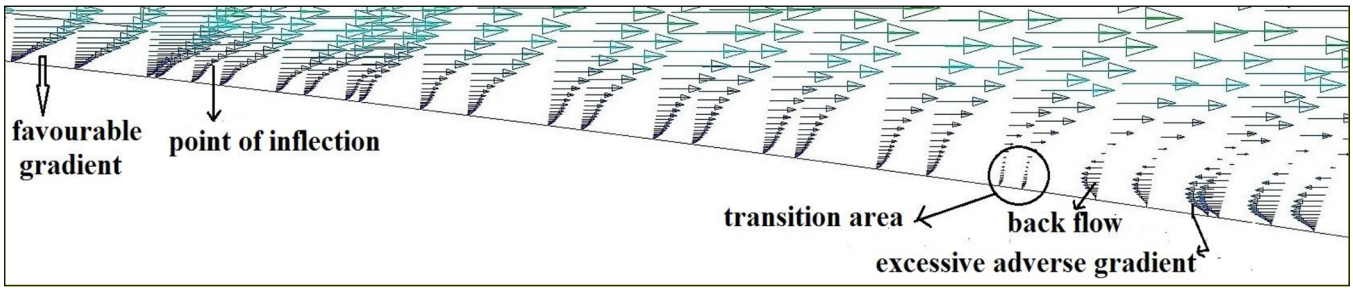

Fig. 25. Closer view of separation zone of Baseline NACA 0015 model.

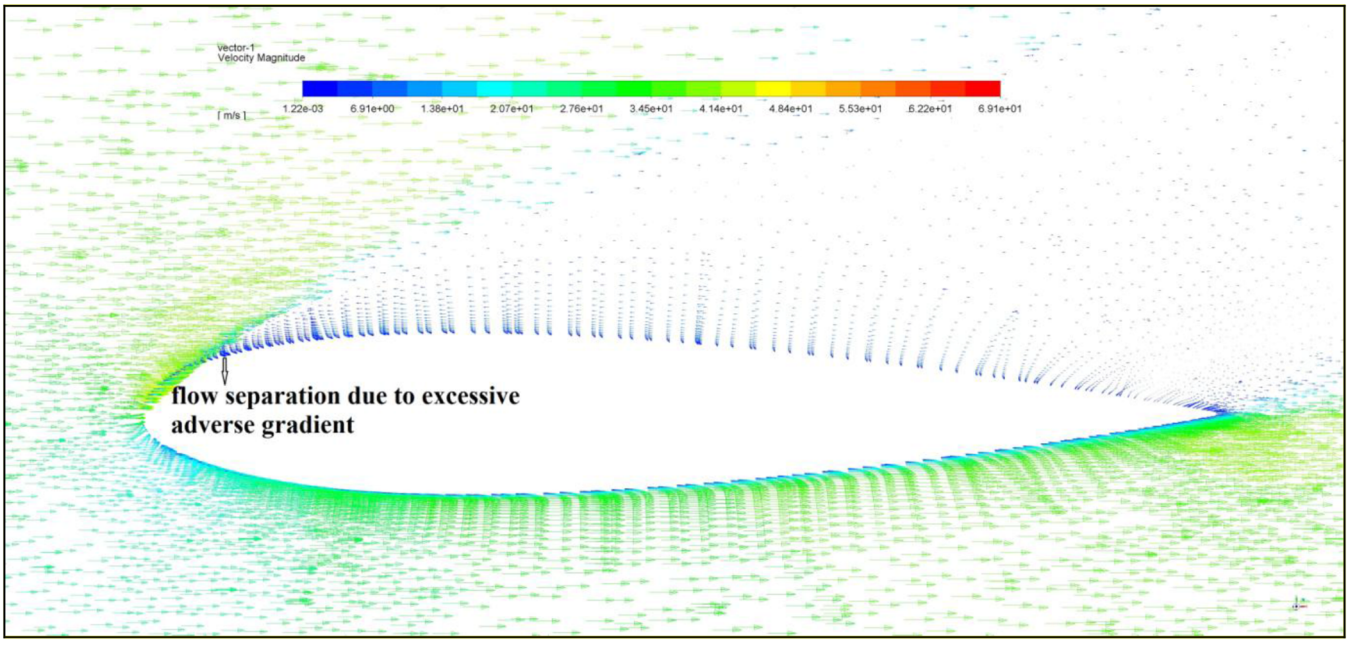

Fig. 26. Velocity vector with boundary layer profile for NACA 0015 model at $\alpha = 15°$.

the wing as highlighted in Figure 26. It is a well-known fact that the early separation is crucial one for the drag divergence that leads to the stall phenomenon at high AoA (Wei et al. [30]). The captured boundary layer clearly shows the flow separation phenomena caused by excessive adverse pressure gradient in the baseline model as well as the trough region of the tubercled model. In the tubercled wing model, the flow first separates behind the trough region (Fig. 27) and the region of flow separation enlarges in size with AoA increments. It is mainly caused by the vortices created by the tubercles that induce upwash behind the trough region which in turn increases the effective AoA.

The peak region of the tubercled model shows the delayed separation because of more favorable pressure gradients. The upwash also thickens the boundary layer behind the trough regions which makes it more prone to separate. Based on earlier investigations, the linear increase is likely to be caused by the gradual flow separation behind the trough regions due to higher adverse pressure gradient. There is a greater adverse pressure gradient behind the troughs of the tubercles than the peak regions as shown in Figures 27 and 28. The pressure gradient downstream of a trough region is more adverse than the peak region of tubercles (Hansen et al. [20]). The downwash effect within the boundary layer over the peak region results in a further delayed onset of stall. Hence, the flow separation starts at about 25% of the chord from the TE as highlighted in Figure 28. The streamwise pressure gradients and boundary layer developments are asymmetrical about the trough centerlines, which is mainly caused by the sweep angle.

3.6 Few industrial applications of HW tubercles

The bio-inspired technology with HW tubercles can be introduced in the new engineering designs to improve their performance characteristics. It is well-known that the tubercles produce pairs of stream wise, counter-rotating vortices (Kristy et al. 2011), and the majority of the investigations have focused on the effects of these tubercled vortices on airfoil and wing performance. However, these

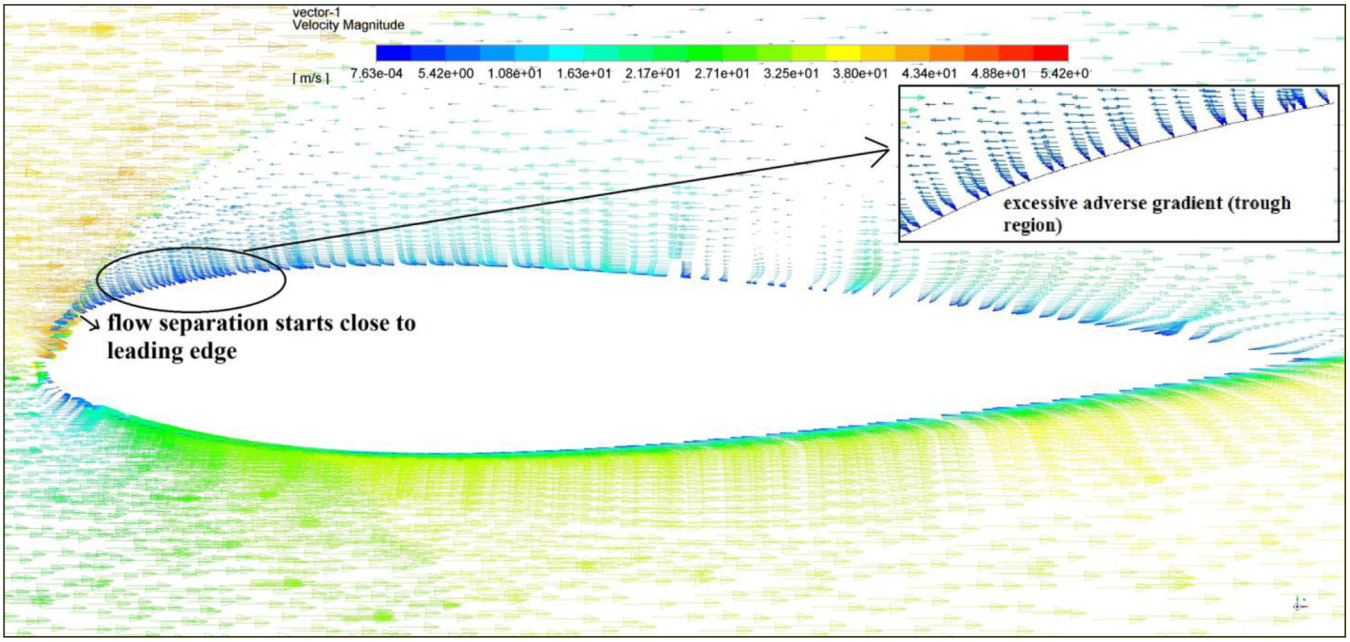

Fig. 27. Velocity vector profile of trough region of HUMP 0015B model at $\alpha = 15°$.

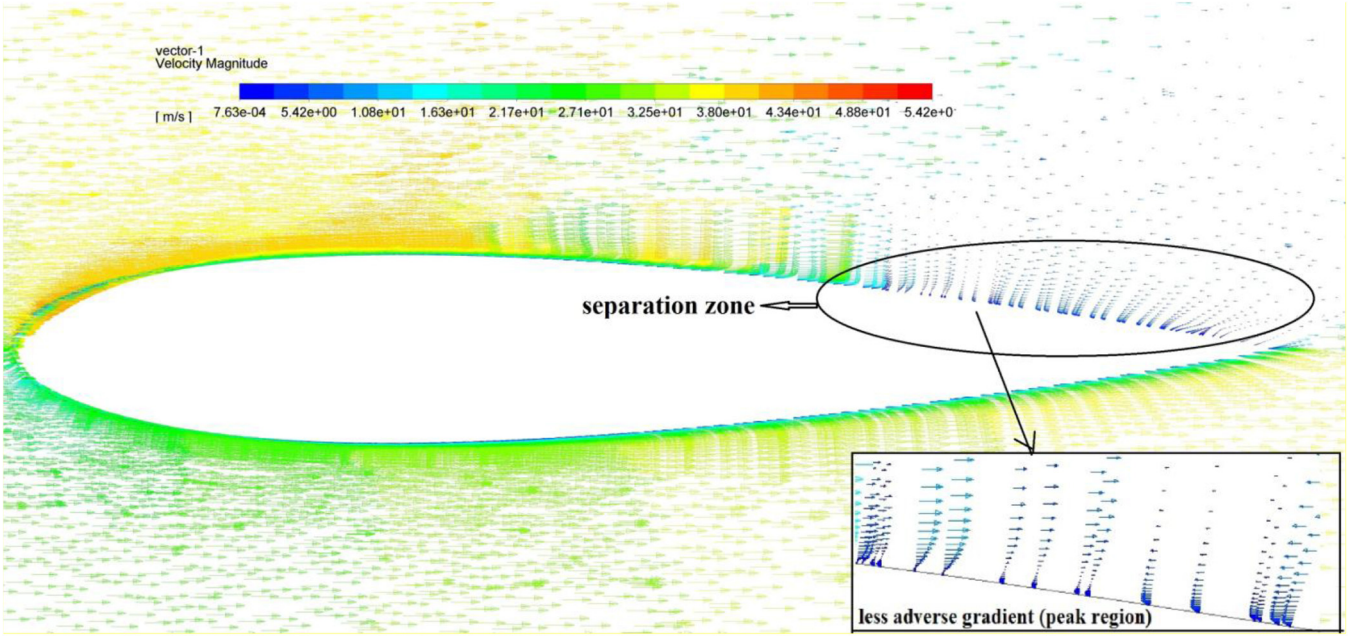

Fig. 28. Velocity vector profile of peak region of HUMP 0015B model at $\alpha = 15°$.

vortices offer significant benefits for enhanced heat transfer through boundary layer thinning, and it facilitates up to a 25% increase in heat transfer. Further, tubercles in the wind turbine blades resulted in a reduction in torsional frequencies while retaining the same plan form area. The reduction in structural frequencies and aerodynamic loads has counteracting effects on fatigue responses. Thus, the tubercles implementation would improve the fatigue life of horizontal axis wind turbine blades (Ng et al. [31]). Application of tubercles has strong influence in the design of hydroplanes where the incorporation of LE tubercles on the hydrofoils provides a balancing force on the yacht and allows it to sail faster (Edel at al. [1]). The implementation of tubercles on the inverted wings in a rear deck of race cars improves the handling performance and accelerating characteristics of automobiles (Bolzon et al. [32]).

4 Conclusions

The aerodynamic performance of swept back wing is analyzed by the proposed Bio-inspired HW tubercles on the LE through systematic optimization of geometric parameters. Aerodynamic surface wall shear flow patterns of six tapered swept-back wing configurations are numerically investigated at a low *Re.* Six designs comprise of two baseline models without tubercles (Baseline NACA0015 & Baseline NACA 4415), two models with tubercles & $\eta = 0.1$ (HUMP 0015 A, HUMP 4415 A), and two more models with tubercles & $\eta = 0.24$ (HUMP 0015 B, HUMP 4415 B) have been considered for this investigation. CFD modelling and analysis is carried out at different AoA ranging from $\alpha = 0°$ to $\alpha = 20°$. The resulting flow structure shows the complicated and asymmetric surface vortex structures that are distributed across the span of the modified wings. The surface vortex structure modifies the distribution of LSB that is formed over both the baseline and tubercled wings. The flow field behind the trough region regularly separates at a lower AoA than the flow over the baseline wing. However, the flow behind the peak region remains attached at a higher AoA.

Aligning the tubercles normal to the LE shows definite improvements in the L/D ratio for AoA range $0° < \alpha < 10°$, as compared with its baseline counterparts. Tubercled wings have improvement in stall behaviour and lift enhancement (particularly for symmetric profile wings) than the baseline models. The tubercled wing model with higher amplitude value gives the increment in C_L and reasonable reduction in C_D at the pre-stall region. This study describes that the wing sweep results in an asymmetrical flow separation pattern about the trough centerline. Similarly, the amplitude and wavelength of tubercles with different ratios, higher *Re* can be studied with different families of airfoils to obtain more practical choices for better aerodynamic performance requirements. Hence, the tubercled configuration has the potential to revolutionize the aerodynamic characteristics of lifting surfaces in the forthcoming days.

Conflict of Interest

The authors declare that they have no conflict of interest in connection with the contents of the article.

Funding

There is no funding source.

Ethical approval

This article does not contain any studies with human participants or animals performed by any of the authors.

Nomenclature

A	Amplitude
α	Angle of attack
Δc	Chord length variation
C_L	Coefficient of lift
C_D	Coefficient of drag
c	Mean chord
η	A/λ
λ	Wavelength
Z	Spanwise ordinate

References

[1] R.K. Edel, H.E. Winn, Observation of underwater locomotion and flipper movement of the Humpback Whale Megaptera Novaeangliae, Marine Biology **48**, 279–287 (1978)
[2] L.N. Cooper, A. Berta, S.D. Dawson, J.S. Reidenberg, Evolution of hyperphalangy and digit reduction in the cetacean manus, The Anatomical Record **290**, 654–672 (2007)
[3] F.E. Fish, J.M. Battle, Hydrodynamic design of the humpback whale flipper, Journal of Morphology **225**, 51–60 (1995)
[4] E.F. Frank, W.W. Paul, M.M. Mark, E.H. Laurens, The tubercles on humpback whales' flippers: application of bio-inspired technology, Integrative and Comparative Biology **51**, 203–213 (2011)
[5] L.H. Kristy, M.K. Richard, B.D. Bassam, Performance variations of leading-edge tubercles for distinct airfoil profiles, AIAA Journal **49**, 185–194 (2011)
[6] P. Watts, F.E. Fish, The influence of passive, leading edge tubercles on wing performance, Proceedings of the 12th International Symposium on Unmanned Untethered Submersible Technology (UUST), 2001, UUST01, Autonomous Undersea Systems Inst., Lee, NH
[7] D. Custodio, C.W. Henoch, H. Johari, Aerodynamic characteristics of finite span wings with leading-edge protuberances, AIAA Journal **53**, 1878–1893 (2015)
[8] P.W. Weber, L.E. Howle, M.M. Murray, Computational evaluation of the performance of lifting surfaces with leading-edge protuberances, Journal of Aircraft **48**, 591–600 (2011)
[9] H. Johari, C. Henoch, D. Custodio, A. Levshin, Effects of leading-edge protuberances on airfoil performance, AIAA Journal **45**, 2634–2642 (2007)
[10] A. Corsini, G. Delibra, A.G. Sheard, On the role of leading-edge bumps in the control of stall onset in axial fan blades, Journal of Fluids Engineering **135**, 1–9 (2013)
[11] R. Percy Torro, J.W. Kim, A large-eddy simulation on a deep-stalled aerofoil with a wavy leading edge, Journal of Fluid Mechanics **813**, 23–52 (2017)
[12] M.M. Zhang, G.F. Wang, J.Z. Xu, Aerodynamic control of low-reynolds-number airfoil with leading-edge protuberances, AIAA Journal **51**, 1960–1971 (2013)
[13] A, Skillen, A. Revell, A. Pinelli, U. Piomelli, J. Favier, Flow over a wing with leading-edge undulations, AIAA Journal **53**, 464–472 (2015)

[14] M.D. Bolzon, R.M. Kelso, M. Arjomandi, Force measurements and wake surveys of a swept tubercled wing, Journal of Aerospace Engineering **30**, 1–3 (2017)
[15] Z. Wei, T.H. New, Y.D. Cui, Aerodynamic performance and surface flow structures of leading-edge tubercled tapered swept-back wings, AIAA Journal **56**, 423–431 (2018)
[16] M.D. Bolzon, R.M. Kelso, M. Arjomandi, Formation of vortices on a tubercled wing, and their effects on drag, Aerospace Science and Technology **56**, 46–55 (2016)
[17] M.M. Murray, D.S. Miklosovic, F.E. Fish, L. Howle, Effects of leading edge tubercles on a representative whale flipper model at various sweep angles, Proceeding of Unmanned Untethered Submersible Technology (UUST), 2005, UUST05, Autonomous Undersea Systems Inst., Lee, NH
[18] P.S. Segre, J. Potvin, D.E. Cade, J. Calambokidis, J. Di Clemente, F.E. Fish, A.S. Friedlaender, W.T. Gough, S.R. Kahane-Rapport, C. Oliveira, S.E. Parks, G.S. Penry, M. Simon, A.K. Stimpert, D.N. Wiley, K.C. Bierlich, P.T. Madsen, J.A. Goldbogen, Energetic and physical limitations on the breaching performance of large whales, Elifescience **51760**, 1–23 (2020)
[19] H. McMorris, Y. Kallinderis, Octree-advancing front method for generation of unstructured surface and volume meshes, AIAA Journal **35**, 976–984 (1997)
[20] K.L. Hansen, N. Rostamzadeh, R.M. Kelso, B.B. Dally, Evolution of stream wise vortices generated between leading edge tubercles, Journal of Fluid Mechanics **788**, 730–766 (2016)
[21] N. Rostamzadeh, K.L. Hansen, R.M. Kelso, B.B. Dally, The formation mechanism and impact of streamwise vortices on NACA 0021 airfoil's performance with undulating leading edge modification, Physics of Fluids **107101** (2014)
[22] C. Cai, Z. Zuo, S. Liu, Y. Wu, Numerical investigations of hydrodynamic performance of hydrofoils with leading edge protuberances, Advances in Mechanical Engineering **7**, 1–11 (2015)
[23] V.T. Gopinathan, J. Bruce Ralphin Rose, V. Gokul, K. Kamalahasan, Numerical investigation of the effect of leading edge Tubercles at low Reynolds number, Proceedings of International Heat and Mass Transfer Conference (IHMTC), 2017, pp. 1055–1059
[24] A. Skillen, A. Revell, A. Pinelli, U. Piomelli, J. Favier, Flow over a wing with leading-edge undulations, AIAA Journal **53**, 464–472 (2015)
[25] D.S. Miklosovic, M.M. Murray, L.E. Howle, F.E. Fish, Leading edge tubercles delay stall on humpback whale flippers, Physics of Fluids **16**, 39–42 (2004)
[26] M.D. Bolzon, R.M. Kelso, M. Arjomandi, Parametric study of the effects of a tubercle's geometry on wing performance through the use of the lifting-line theory, 54th AIAA Aerospace Sciences Meeting, 2016, California, USA
[27] K. Bang, J. Kim, S. Lee et al., Hydrodynamic role of longitudinal dorsal ridges in a leatherback turtle swimming. Science Reports **6**, 34283 (2016)
[28] A.S.H. Lau, S. Haeri, J.W. Kim, The effect of wavy leading edges on aerofoil-gust interaction noise, Journal of Sound and Vibration **24**, 6234–6253 (2013)
[29] M.D. Bolzon, R.M. Kelso, M. Arjomandi, Force measurements and wake surveys of a swept tubercled wing, Journal of Aerospace Engineering **30**, 04016085 (2017)
[30] Z. Wei, T.H., New, L. Lian, Y.N. Zhang, Leading-edge tubercles delay flow separation for a tapered swept-back wing at very low Reynolds number, Ocean Engineering **181**, 173–184 (2019)
[31] B.F. Ng, T.H. New, R. Palacios, Bio-inspired leading-edge tubercles to improve fatigue life in horizontal axis wind turbine blades, Thirty fifth wind energy symposium, Texas, 1381, 2017
[32] M.D. Bolzon, R.M. Kelso, M. Arjomandi, Tubercles and their applications, Journal of Aerospace Engineering **29**, 1–10 (2015)

Cite this article as: V.T. Gopinathan, J. Bruce Ralphin Rose, M. Surya, Investigation on the effect of leading edge tubercles of sweptback wing at low reynolds number, Mechanics & Industry **21**, 621 (2020)